Nanoscale

Accepted Manuscript

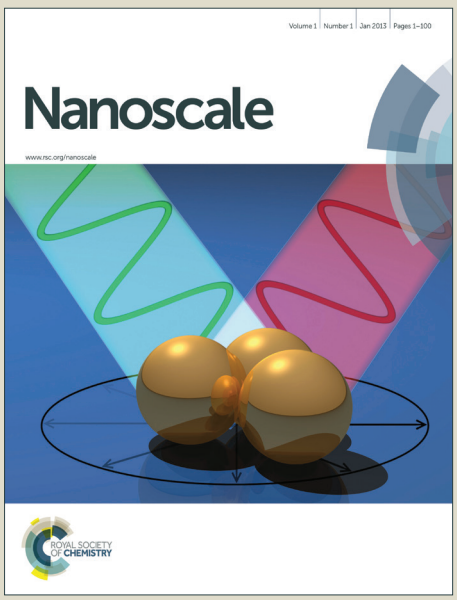

ROYAL SOCIETY OF CHEMISTRY

www.rsc.org/nanoscale

Journal Name

RSCPublishing

COMMUNICATION

Superwetting hierarchical porous silica nanofibrous membranes for oil/water microemulsion separation

Cite this: DOI: 10.1039/x0xx00000x

Shan Yang,[†ab] Yang Si,[†ab] Qiuxia Fu,[ab] Feifei Hong,[ab] Jianyong Yu,[b] Salem S. Al-Deyab,[c] Mohamed El-Newehy[cd] and Bin Ding*[ab]

Received 00th January 2012,
Accepted 00th January 2012

DOI: 10.1039/x0xx00000x

www.rsc.org/

Novel flexible, thermally stable and hierarchical porous silica nanofibrous membranes with superhydrophilicity and underwater superoleophobicity were prepared by a facile in situ synthesis method, which can effectively separate oil-in-water microemulsions solely driven by gravity, with an extremely high flux of 2237 L m^{-2} h^{-1}.

With increasing environmental awareness and tighter regulations, novel strategies to separate oil from industrial wastewaters, polluted oceanic waters, and oil-spill mixtures, especially in the presence of surfactants, are highly desired.[1-3] Conventional methods such as oil skimmers, centrifuges, flotation, depth filters, and coalescers are available for separation of immiscible oil/water mixtures, but are not effective for emulsified oil/water mixtures, especially not for surfactant stabilized microemulsions (droplet sizes < 20 μm).[3-6] Membrane-based technologies have aroused great attention for the separation of emulsions, because they are relatively cost-effective and available for a wide range of industrial effluents.[7, 8] In spite of the advantages, these polymer dominated separation membranes generally suffer from low flux (~ 300 L m^{-2} h^{-1}), high driven pressure (> 10 kPa), poor thermal stability (< 180 °C), as well as serious fouling and plugging because of surfactant adsorption.[9-11] In this communication, we present a robust methodology for creating superhydrophilic and underwater superoleophobic silica nanofibrous (SNF) membranes with a hierarchical porous structure by the combination of nanofibers with in situ polymerization. The premise for our design is that, the SNF membranes can effectively separate micro-size surfactant stabilized oil-in-water emulsions solely driven by gravity, with high separation efficiency. Most importantly, the membranes exhibit the high flux, robust mechanical strength, high thermal stability, and ease of cycling for long-term use.

We designed the SNF separation membranes based on three criteria: (1) the membranes must be superhydrophilic and underwater superoleophobic, (2) the membranes must be mechanically robust and thermally stable, and (3) the oil/water microemulsions must be completely demulsified and separated as they move through the membranes. Scheme 1 describes the synthesis pathway. The pristine electrospun SNF membranes were used as the template to construct the separation membranes, and an aldehyde benzoxazine, namely 3-phenyl-3,4-dihydro-2H-benzooxazine-6-carbaldehyde (BA-CHO) was

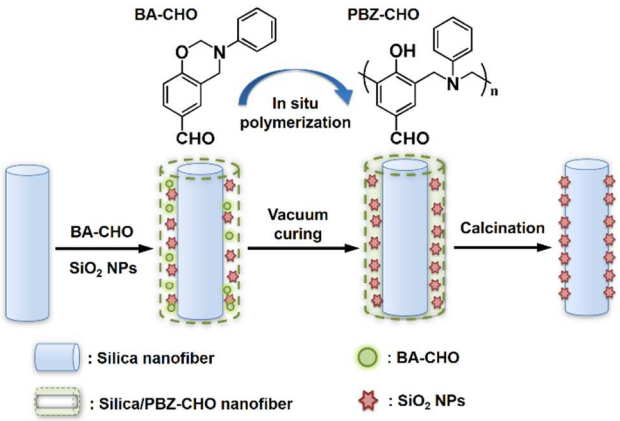

Scheme 1 Illustration of the synthesis of hierarchical porous SNF membranes by combining the nanofibers with in situ polymerization.

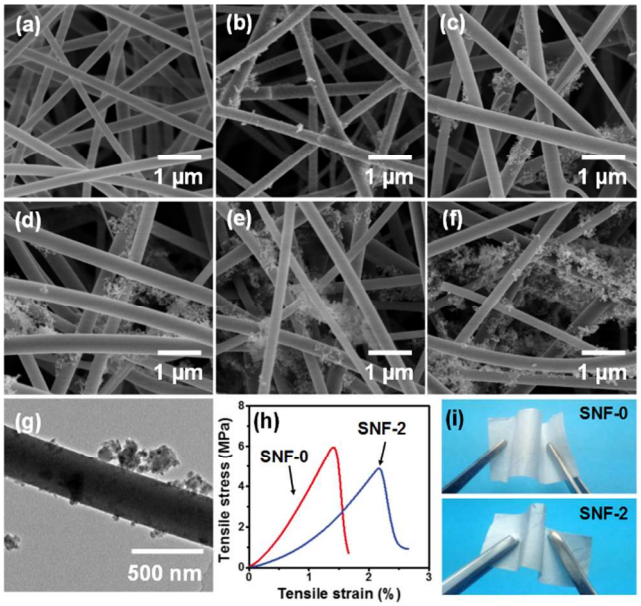

Fig. 1 FE-SEM images of (a) SNF-0, (b) SNF-0.01, (c) SNF-0.1, (d) SNF-0.5, (e) SNF-1, and (f) SNF-2 membranes. (g) TEM image of SNF-2 membranes. (h) Tensile stress-strain curves of SNF-0 and SNF-2 membranes. (i) Optical photographs show the robust flexibility of SNF-0 and SNF-2 membranes.

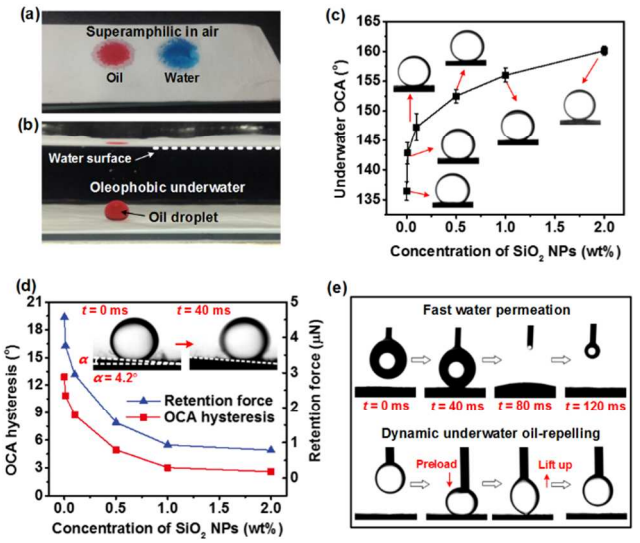

Fig. 2 (a) Droplets of oil (dyed red) and water (dyed blue) on the SNF-0 membranes in air. (b) Photograph of an underwater oil droplet (dyed red) on the SNF-0 membranes. (c) Variations of the underwater OCA of SNF membranes with increasing of SiO_2 NPs concentrations. (d) The underwater OCA hysteresis and retention force as a function of SiO_2 NPs concentrations, inset shows the oil droplet (10 μL) sliding at a low angle of 4.2° on the surface of SNF-2 membranes. (e) Photographs of dynamic measurements of water permeation (top) and underwater oil-repelling (bottom) on the surface of SNF-2 membranes.

used as the novel in situ polymerization monomers. SiO_2 nanoparticles (SiO_2 NPs) were introduced into the membranes to create nano-scale roughness. The silica nanofibers were first fabricated by the calcination of electrospun tetraethyl orthosilicate/poly(vinyl alcohol) hybrid nanofibers. Following, they were dipped in the acetone solutions containing BA-CHO (1 wt%) and SiO_2 NPs with various concentrations (0.01, 0.1, 0.5, 1, and 2 wt%), and dried in an oven for 30 min. Subsequently, the in situ polymerization of BA-CHO was carried out at 220 °C in vacuum for 1 h, leading to the formation of a polybenzoxazine (PBZ-CHO) layer containing SiO_2 NPs on the fiber surface. Finally, the membranes were calcined at 850 °C under N_2 flow to generate the hierarchical porous SNF membranes. The obtained samples with the SiO_2 NPs concentration of x wt% were denoted as SNF-x, and the pristine SNF membranes were denoted as SNF-0, as summarized in Table S1.

As shown in Fig. 1a, the pristine SNF-0 membranes exhibited a randomly oriented nonwoven structure with an average diameter of 230 nm. Upon curing at 220 °C, the BA-CHO monomers gradually polymerized and converted to the Mannich bridge cross-linked structure, finally generating the cured thermosetting PBZ-CHO layer on the fiber surface. Evidence for the formation of PBZ-CHO also came from FT-IR spectral analysis (Fig. S3), the characteristic peak around 1656 cm^{-1} was assigned to the stretching vibration of C=O, and the peaks around 1608 and 1503 cm^{-1} belonged to the skeletal vibration of benzene ring.[12] During the following calcination, the PBZ-CHO layer was gradually decomposed. A spot of carbon (1.12 wt%) was found in the resultant SNF membranes based on the energy-dispersive X-ray spectroscopy (EDX) analysis (Fig. S4), which could be attributed to the incomplete decomposition of PBZ-CHO.[13] It should be noted that this in situ generated carbon could effectively bond the SiO_2 NPs on the fibers, and also slightly increased the diameter of the fibers (Table S1). As shown in Figs. 1b-g, the majority of SiO_2 NPs were well-positioned on the surface of nanofibers, and only a small amount of SiO_2 NPs were presented among the voids of nanofibers, indicating the effective construction of hierarchical roughness. Moreover, in dramatic contrast to the brittle nature of traditional inorganic nanofibers, the SNF-0 and SNF-2 membranes (taken SNF-2 as an example) exhibited good mechanical properties with tensile strength of 6.01 and 5.06 MPa, respectively (Fig. 1h). Fig. 1i presented that these membranes could be facilely bended and folded, and no cracks were observed (see also Movie S1 and S2 for SNF-0 and SNF-2 membranes, respectively), highlighting their robust flexibility.

The pristine SNF-0 membranes have a surface layer of hydrophilic silanol groups, leading to a high surface energy of more than 40 mN m^{-1}.[14] Thus the SNF-0 membranes have shown superamphilicity in air with both the water contact angle and oil (dichloromethane) contact angle (OCA) of 0° (Fig. 2a). Interestingly, the oleophobicity appeared immediately for SNF-0 membranes after being immersed in water, as shown in Fig. 2b. This was due to the significantly higher adhesion work of water than that of oil, which could be calculated according to the Young Dupré's Equation: $W_{ad} = \gamma_{lv}(1 + \cos\theta_{lv})$, where the W_{ad} is the adhesion work, the γ_{lv} is the surface tension of liquid, and the θ_{lv} is the relevant liquid contact angle.[15] The estimated adhesion work of water and oil (dichloromethane) for SNF-0 membranes were 144 and 46 mN m^{-1}, respectively, which indicated that the infiltrated water in membranes was hard to be replaced by oil, resulting the robust underwater oleophobicity. Moreover, the intrinsic lyophobicity of a

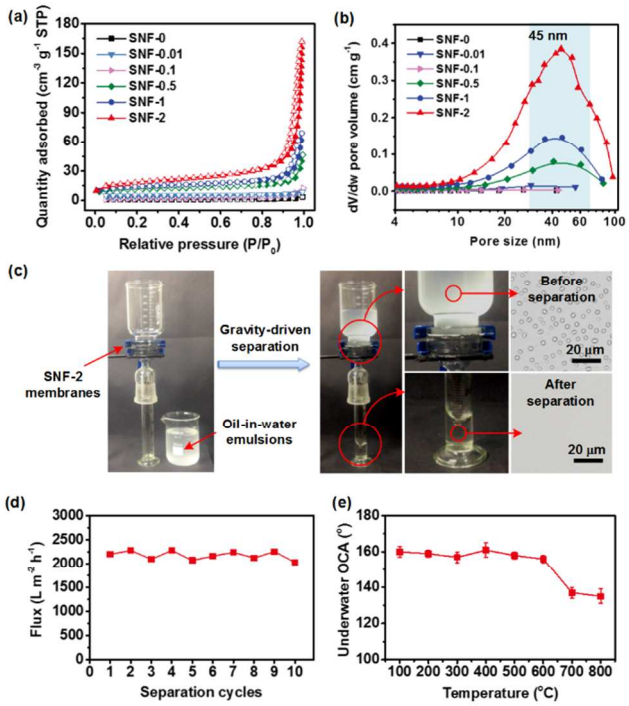

Fig. 3 (a) N_2 adsorption-desorption isotherms and (b) BJH PSD analysis of the relevant SNF membranes. (c) Photographs showed the facile gravity-driven separation of oil-in-water microemulsions using SNF-2 membranes. (d) Changes of the flux with increasing separation cycles using SNF-2 membranes. (e) Underwater OCA of the SNF-2 membranes after calcination in air at different temperatures for 10 min.

surface could be improved by being textured with multiple scaled roughness according to the Cassie model.[16, 17] This law was also applied to the underwater oleophobicity since the trapped air in pores was equally substituted by water. As shown in Fig. 2c, with the addition of SiO_2 NPs, a noteworthy increase of underwater OCA to 161° could be observed, confirming the underwater superoleophobicity of as-prepared SNF membranes. This prominent superhydrophilic and underwater superoleophobic property ensures water-layer formation on the membrane surface and avoids direct contact between oil and membrane surface during separation, which could effectively enhance the antifouling property of the membranes.

Another significant wetting properties to study the contact behaviour are the OCA hysteresis (the difference between the advancing and receding contact angles of a moving droplet) and sliding angle (the surface tilt required for droplet motion), which directly characterize resistance to mobility.[18, 19] As shown in Fig. 2d, the underwater OCA hysteresis decreased regularly with the increasing of SiO_2 NPs concentrations, achieving the lowest value of 2.6° for the SNF-2 membranes. Such a low value of hysteresis revealed that the oil could not penetrate into the membranes to large extent and sat on the asperities of the surface with the minimum liquid-solid adhesion, thus the oil droplets are able to roll off the surface easily with a minute sliding angle of 4.2°, as demonstrated in the inset of Fig. 2d. Based on the measured OCA hysteresis and droplet volume (10 μL), the estimated liquid adhesion forces of the as-prepared SNF membranes were ranging from 4.57 to 0.78 μN (See details in the Support Information).[18, 20] This performance is obviously better than the state-of-the-art lotus-leaf-inspired omniphobic surfaces, whose liquid retention forces are of the order of 5 μN.[16, 21]

To investigate the dynamic wetting behaviour of water on the membranes, a high-speed camera system was used to examine the adhesion and permeating process of a liquid droplet. As shown in Fig. 2e (top), when a 3 μL of water droplet contacted the SNF-2 membranes, it permeated in the membranes quickly and a nearly zero contact angle was reached. The whole process was completed within 120 ms, suggesting the prominent property of the SNF-2 membranes for water wetting. Simultaneously, the membranes behaved as an underwater superior oil-repelling property. Fig. 2e (bottom) exhibited the photographs of a 3 μL of oil (dichloromethane) droplet touching and leaving the SNF-2 membrane surface. The droplet was forced to sufficiently contact the membrane surface with a distinct compression, and it was then lifted up. The corresponding photographs showed almost no deformation when the droplet left the membrane surface, thus confirming the extremely low oil adhesion force.

The systematic design of membranes for emulsion separation requires the optimization of two important structure characteristics: pore size distribution (PSD), which affects the rate of permeation of one phase (separation flux) through the membranes; the specific surface area, which defines the demulsification efficiency by the irreversible adsorption of surfactants.[22,23] Therefore, to provide insight into the hierarchical porous structure, the N_2 adsorption-desorption analyses were performed for the relevant SNF membranes. As shown in Fig. 3a, the relevant isotherms exhibited the isotherm of type IV with a series of typical adsorption behaviours including monolayer adsorption, multilayer adsorption and capillary condensation, revealing characteristics of mesopores within as-prepared membranes.[24, 25] The narrow H1 hysteresis loop at the region of P/P_0 > 0.8 revealed that the mesopores were open.[26, 27] Significantly, the calculated Brunauer-Emmett-Teller (BET) surface area increased dramatically from 3.16 to 62.48 m^2 g^{-1} (Table S1), indicating the major contributing role of SiO_2 NPs on deciding the surface area. Moreover, PSD analysis was achieved by employing the Barrett-Joyner-Halenda (BJH) method (Fig. 3b). The SNF membranes exhibited a typical polydisperse porous structure and a primary PSD in the range of 20-80 nm, and well-developed peaks centered at 45 nm could be observed, which matched well with the maximum size of SiO_2 NPs. In addition, the capillary flow method was used to analyse the macroporous structure of the SNF membranes, as demonstrated in Fig. S5. The relevant membranes exhibited relatively centered peaks and ranged in 1.5–2 μm. With the increasing of SiO_2 NPs concentration, the mean pore size slightly decreased from 2.03 to 1.60 μm, which was because that the SiO_2 NPs were mainly positioned on the surface of nanofibers rather than in the voids of nanofibers. The hierarchical porous structure originated from the synergistic effect of mesoporosity and macroporosity indicated that obviously improved separation performances should be expected.

To test the separation capability of the as-prepared membranes, a surfactant-stabilized (Tween 80) oil (petroleum ether was taken as an example)-in-water microemulsion with an average droplet size of 3.82 μm was prepared (Fig. S6). As shown in Fig. 3c, 200 mL of microemulsions were poured onto the SNF-2 membranes, pure water immediately permeated through the membranes and dropped into the below cylinder (see also Movie S3). Meanwhile, the emulsion oil droplets demulsified once touching the membranes and oil was retained above. No external driven force was used during the fast separation process, only their own weight. The optical microscopic images of collected filtrate showed that no droplet was observed in the collected filtrate in the whole image, indicating the high effectiveness for separating microemulsions. Significantly, the SNF-2 membranes exhibited a promising separation flux of 2237±180 L m^{-2} h^{-1}, which was an order of magnitude higher than that of pressure driven commercial separation membranes. The antifouling performance presented in Fig. 3d indicated outstanding reusability with nearly no flux decrease upon 10 cycles, revealing the excellent antifouling property of these membranes for long-term use. Moreover, benefiting from the inorganic character, the SNF-2 membranes exhibited the remarkable thermal stability with no change in the underwater OCA even after the annealing treatment at 600 °C for 10 min (Fig. 3e), thereby implying the potential application of the membranes towards extreme conditions. By further increasing the annealing temperature up to 700 °C, the OCA decreased to 135°, similar with the pristine SNF-0 membranes, which was due to the complete decomposition of carbon adhesive and the following break of the nano-scale rough structure.

In summary, we have demonstrated an in situ strategy for fabricating superhydrophilic and underwater superoleophobic SNF membranes that allow effective separation of surfactant-stabilized oil-in-water microemulsions. With prominent selective superwettability, high specific surface area, and mesoporosity, the as-prepared SNF-2 membranes exhibited high separation efficiency and an extremely high flux of 2237 L m^{-2} h^{-1}, which was much higher than traditional polymeric separation membranes with similar separation properties. More importantly, the membranes exhibited robust mechanical strength, high thermal stability, good antifouling property, and ease of cycling, which matched well with the requirements for treating the real emulsified wastewater on a mass scale. This work also provided a versatile in situ strategy for further design and development of functional nanofibrous membranes towards various applications.

Acknowledgements

This work is supported by the National Natural Science Foundation of China (No. U1232116 and 51322304), the Program for New Century Talents of the University in China, the Fundamental Research Funds for the Central Universities, and the “DHU Distinguished Young Professor Program”. The authors extend their appreciation to the Deanship of Scientific Research at King Saud University for funding the work through the international research group project no. IRG14-25.

Notes and references

[a] Key Laboratory of Textile Science & Technology, Ministry of Education, College of Textiles, Donghua University, Shanghai 201620, China. E-mail: binding@dhu.edu.cn.
[b] Nanomaterials Research Center, Modern Textile Institute, Donghua University, Shanghai 200051, China
[c] Petrochemical Research Chair, Department of Chemistry, College of Science, King Saud University, Riyadh 11451, Saudi Arabia
[d] Department of Chemistry, Faculty of Science, Tanta University, Tanta 31527, Egypt
† These authors have contributed equally to this work.
Electronic Supplementary Information (ESI) available: [Detailed synthesis and structural confirmation of BA-CHO, FT-IR and EDX results, Movie S1-S3]. See DOI: 10.1039/c000000x/

1. A. K. Kota, G. Kwon, W. Choi, J. M. Mabry and A. Tuteja, *Nat. Commun.*, 2012, **3**, 1025.
2. Y. Wang, S. Tao and Y. An, *J. Mate. Chem. A* 2013, **1**, 1701-1708.
3. X. M. Tang, Y. Si, J. L. Ge, B. Ding, L. F. Liu, G. Zheng, W. J. Luo and J. Y. Yu, *Nanoscale*, 2013, **5**, 11657-11664.
4. M. Tao, L. Xue, F. Liu and L. Jiang, *Adv. Mater.*, 2014, **26**, 2943-2948.
5. M. W. Lee, S. An, S. S. Latthe, C. Lee, S. Hong and S. S. Yoon, *ACS Appl. Mater. Inter.*, 2013, **5**, 10597-10604.
6. B. M. S. Ferreira, J. B. V. S. Ramalho and E. F. Lucas, *Energ. Fuel.*, 2013, **27**, 615-621.
7. Z. Shi, W. Zhang, F. Zhang, X. Liu, D. Wang, J. Jin and L. Jiang, *Adv. Mater.*, 2013, **25**, 2422-2427.
8. Z. Xue, S. Wang, L. Lin, L. Chen, M. Liu, L. Feng and L. Jiang, *Adv. Mater.*, 2011, **23**, 4270-4273.
9. G. Kwon, A. K. Kota, Y. Li, A. Sohani, J. M. Mabry and A. Tuteja, *Adv. Mater.*, 2012, **24**, 3666-3671.
10. W. Zhang, Y. Zhu, X. Liu, D. Wang, J. Li, L. Jiang and J. Jin, *Angew. Chem. Int. Ed.*, 2014, **53**, 856-860.
11. Y. W. Shang, Y. Si, A. Raza, L. P. Yang, X. Mao, B. Ding and J. Y. Yu, *Nanoscale*, 2012, **4**, 7847-7854.
12. N. N. Ghosh, B. Kiskan and Y. Yagci, *Prog. Polym. Sci.*, 2007, **32**, 1344-1391.
13. Y. Si, T. Ren, B. Ding, J. Yu and G. Sun, *J. Mater. Chem.*, 2012, **22**, 4619-4622.
14. E. Papirer, *Adsorption on silica surfaces*, CRC Press, 2000.
15. S. Agarwal, V. Arnim, T. Stegmaier, H. Planck and A. Agarwal, *Sep. Purif. Technol.*, 2013, **107**, 19-25.
16. X. Wang, B. Ding, J. Yu and M. Wang, *Nano Today*, 2011, **6**, 510-530.
17. Y. P. Li, W. W. Xiao, K. Xiao, L. Berti, J. T. Luo, H. P. Tseng, G. Fung and K. S. Lam, *Angew. Chem. Int. Ed.*, 2012, **51**, 2864-2869.
18. T. S. Wong, S. H. Kang, S. K. Y. Tang, E. J. Smythe, B. D. Hatton, A. Grinthal and J. Aizenberg, *Nature*, 2011, **477**, 443-447.
19. X. Wang, B. Ding, G. Sun, M. Wang and J. Yu, *Prog. Mater. Sci.*, 2013, **58**, 1173-1243.
20. C. G. L. Furmidge, *J. Colloid Sci.*, 1962, **17**, 309-324.
21. J. L. Wang, A. Raza, Y. Si, L. X. Cui, J. F. Ge, B. Ding and J. Y. Yu, *Nanoscale*, 2012, **4**, 7549-7556.

22. S. Tao, Y. Wang and Y. An, *J. Mater. Chem.*, 2011, **21**, 11901-11907.
23. S. Tao and Y. Wang, *Int. Nano Lett.*, 2014, **4**, 102.
24. Z. Zhu, L. Zhang, J. Y. Howe, Y. Liao, J. T. Speidel, S. Smith and H. Fong, *Chem. Commun.*, 2009, 2568-2570.
25. Y. Si, T. Ren, Y. Li, B. Ding and J. Yu, *Carbon*, 2012, **50**, 5176-5185.
26. N. A. M. Barakat, B. Kim, C. Yi, Y. Jo, M. H. Jung, K. H. Chu and H. Y. Kim, *J. Phys. Chem. C*, 2009, **113**, 19452-19457.
27. B. Y. Li, B. B. Jiang, D. J. Fauth, M. L. Gray, H. W. Pennline and G. A. Richards, *Chem. Commun.*, 2011, **47**, 1719-1721.